Structural Investigation of Monolayers Prepared by Deposition of $(CH_3S)_2$ on the (111) Face of Single-Crystal Gold

Mehmet F. Danışman, Loredana Casalis,† Gianangelo Bracco,‡ and Giacinto Scoles*

Department of Chemistry, Princeton University, Princeton, New Jersey 08544

Received: March 19, 2002; In Final Form: June 19, 2002

Although self-assembled monolayers made of long chains of *n*-alkanethiols $[CH_3(CH_2)_{n-1}SH]$ on Au(111) have been extensively studied in the past, the driving forces behind the appearance of the $(3 \times 2\sqrt{3})$ superlattice observed at full coverage are still not completely understood. To focus on the role played by the sulfur headgroup minimizing the interactions between chains and to prevent a possible X-ray-induced damage, we have carried out a He atom diffraction study of the adsorption of the shortest ($n = 1$) thiol radical, obtained by dissociative adsorption of $(CH_3S)_2$, on the Au(111) surface. Contrary to current literature reports, domains of the hexagonal $(\sqrt{3} \times \sqrt{3})R30°$ structure are observed to convert into the well-ordered $(3 \times 2\sqrt{3})$ superstructure after annealing times of a few hours. The observation of peaks forbidden by the $(3 \times 2\sqrt{3})$ model proposed by Fenter et al. (Fenter, P.; Eberhardt, A.; Eisenberger, P. *Science* **1994**, *266*, 1216) suggests a distortion of the symmetry of the unit cell. The observed chemisorption and physisorption energies were in good agreement with the literature.

Introduction

Self-assembled monolayers (SAMs) of thiol-functionalized molecules on gold have been studied extensively because of their role as model systems for better understanding the self-organization of matter in two dimensions.[1,2] Their numerous technological applications in corrosion inhibition[3] and the nanofabrication of electronic devices,[4] sensors,[5] and nonlinear optics[6] are another reason for the considerable attention that these systems have enjoyed during the past 10 years.

Among all SAMs alkanethiols $[CH_3(CH2)_{n-1}SH]$ on Au(111) are one of the best studied systems. In early scanning probe microscopy studies on alkanethiols, Porter and his co-workers observed a hexagonal $(\sqrt{3} \times \sqrt{3})R30°$ lattice structure for chains with $n = 2$ and 4−17 using both atomic force microscopy (AFM)[7] and scanning tunneling microscopy (STM).[8] Using low-energy electron diffraction (LEED), Dubois et al.[9] observed the same structure for $n < 3$, whereas for $4 < n < 12$, they reported larger unit cells $[(m\sqrt{3} \times \sqrt{3})R30°$, where m is an integer between 4 and 6 depending on the chain length]. Both of the above-mentioned groups assigned the 3-fold-hollow site as the preferred adsorption site. Aside from the observation of the diffraction peaks due to the $(\sqrt{3} \times \sqrt{3})R30°$ hexagonal lattice, additional peaks were observed by means of X-ray diffraction (XRD),[10,11] low-energy atom diffraction (LEAD),[12−14] and STM techniques[15,16] for alkanethiols with $n > 8$ that indicated the presence of a $(3 \times 2\sqrt{3})$ superlattice. Fenter et al.[10] attributed the origin of the superlattice to headgroup−substrate interactions, and proposed a unit cell with two pairs of inequivalent sulfur atoms, each pair having one atom on the 3-fold-hollow site and one on the bridge site at a relatively short distance from each other. The same group addressed the effect of chain length on 2-D packing structure for chains of n between 10 and 30.[11] Although they observed two different regimes for $n < 14$ and $n > 16$ that were distinguished by the tilt angle of the chains, caused by the balance between the interchain and substrate−headgroup interactions, they observed the $(3 \times 2\sqrt{3})$ superlattice for all of the alkanethiols investigated in their studies.

In other studies concentrating on shorter chains ($n < 6$) and employing microscopy techniques, several striped phases have been reported. Dishner et al.[17] reported, in addition to a $(3 \times 2\sqrt{3})$ structure, a $(2\sqrt{3} \times \sqrt{3})R30°$ striped phase for methanethiol SAMs. Voets et al.[18] reported striped phases for $n = 4-6$ with unit cells $(p \times \sqrt{3})$ (with $p = 3$ for $n = 4$ and 5 and $p = 4$ for $n = 6$) on Au(111).

Recently, several groups have investigated the alkanethiol headgroup−substrate interaction from a theoretical point of view. In these studies, which employ density functional theory (DFT) methods, contradictory results have been reported for the adsorption site of methanethiolate on Au(111). Yourdshahyan et al.[19] and Gronbeck et al.[20] indicate the fcc 3-fold-hollow site as the most stable one,; however, Hayashi et al.[21] and Vargas et al.[22] found the bridge site as the most stable adsorption site. Vargas et al. were also able to identify a $(3 \times 2\sqrt{3})$ superlattice with the sulfur atoms sitting on two different bridge sites that was energetically indistinguishable from the $(\sqrt{3} \times \sqrt{3})R30°$ hexagonal lattice at full coverage. The behavior of dimethyl disulfide on Au(111) has also been investigated by the above-mentioned groups. The common result of all of these studies was the dissociative adsorption of dimethyl disulfide on the Au(111) surface. The dissociative adsorption of dimethyl disulfide on Au(111) at room temperature has been also reported in several experimental studies where TPD,[23] AFM,[24] XPS,[23,25] and STM[26] techniques have been employed. Although there are still some controversial results in the literature regarding this issue, it is generally observed that the structures obtained adsorbing either symmetric dialkyl disulfides or alkanethiols are indistinguishable from each other (ref 2 and references therein).

* To whom all correspondence should be addressed. E-mail: scoles@princeton.edu (G.S.).

† Permanent address: Sincrotrone Trieste, Trieste, Italy. E-mail: lcasalis@princeton.edu.

‡ Permanent address: INFM and Department of Physics, University of Genova, Italy. E-mail: bracco@fisica.unige.it.

10.1021/jp0257911 CCC: $22.00
Published on Web 10/18/2002

Unfortunately, the inconsistencies among both experimental and theoretical studies results in an incomplete picture for the short chain alkanethiols. To contribute to a better understanding of this subject, we have studied the structure of methanethiolate on Au(111) as obtained by dissociative adsorption of dimethyl disulfide (DMDS) using LEAD. Our results clearly indicate the presence of a $(3 \times 2\sqrt{3})$ superstructure at saturation coverage. In the absence of quantitative intensity calculations (presently in progress), we cannot at this time reach any conclusion on the nature of the binding site. Intensity calculations for He beam diffraction in such a highly corrugated system, with peak-to-valley corrugations on the order of 1 Å, have thus far been unfeasible because of convergency problems in the solutions of the close-coupled multichannel scattering problem. As new, faster programs have recently become available,[27] these type of calculations are expected to deliver height information for the CH_3 groups and therefore to lend insight also into the positions of the sulfur atoms.

Experimental Section

Here, we will focus on the main characteristics of the He atom diffraction apparatus used in our experiments. For a more detailed description, the reader is referred to previous publications.[28,29] A monoenergetic helium beam was produced by supersonic expansion from a He source that was kept at 70 K. The energy of the He beam was about 14 meV, and it had a dispersion of ~2%. The beam was collided with the surface at a constant incidence angle of 60° ± 0.5°, and the resulting diffraction pattern was detected by rotating a liquid-helium-cooled bolometer (kept at 1.6 K by pumping on the liquid helium) around the surface in a horizontal plane containing the incident beam and the normal to the surface. The angular distribution of the scattered atoms was transformed to momentum space by using the equation

$$\Delta K_{||} = k_i(\sin\theta_f - \sin\theta_i)$$

where $\Delta K_{||}$ is the parallel momentum transfer; k_i and θ_i are the incident wave vector and angle, respectively; and θ_f indicates the angular position of the detector. Because there is widespread agreement on the fact that the CH_3S over layer is commensurate with the Au(111) mesh, the incident wave vector, k_i, was calibrated using the (−2, 0) and (−4, 0) diffraction peaks of the $(3 \times 2\sqrt{3})$ superlattice [coincident with the first- and second-order peaks of the $(\sqrt{3} \times \sqrt{3})$R30° hexagonal lattice; see Figure 7b for a detailed description] of the methanethiolate layer and calculated to be 5.1 $Å^{-1}$ at the source temperature of 70 K. The diffraction geometry is shown in Figure 1a, where $K_f - K_i$ represents the parallel momentum transfer $\Delta K_{||}$.

The detector, the crystal, and the doser were housed in two concentric radiation shields cooled by liquid nitrogen (Figure 1b). This shield, in conjunction with the cryopumping action of the liquid-helium 1.6 K cryostat, provides for extremely (actually, immeasurably) low pressures for all gases but H_2 and He in the scattering environment. The crystal manipulator has three degrees of freedom for the crystal and one for the detector, which correspond to the polar (θ_i), azimuthal (ϕ), and tilt (χ) angles of the crystal and the polar rotation of the detector (θ_f). θ_i determines the helium beam incidence angle and was kept constant during the course of this study. The high sensitivity of the bolometer detector at low crystal temperatures (the minimum detectable flux is $\sim 5 \times 10^8$ atoms/s at a 70 K primary beam source temperature) enables very efficient detection of diffracted helium, as the primary beam flux of $\sim 4 \times 10^{14}$ He atoms/s can be detected with a signal-to-noise ratio (S/N) of 5000. However, at elevated sample temperatures, two effects cause a reduction of the detected intensity. The first is attenuation of the helium elastic diffraction signal caused by the thermal motion of the surface atoms (Debye−Waller effect). The second is the radiation emanating from the crystal, which heats the bolometer, thereby shifting its working point and substantially reducing its sensitivity. Although specular reflection can still be detected up to 550 K (crystal substrate temperature), diffraction patterns cannot be observed above 150 K. For this reason, all diffraction measurements were performed at a crystal temperature of 40 K.

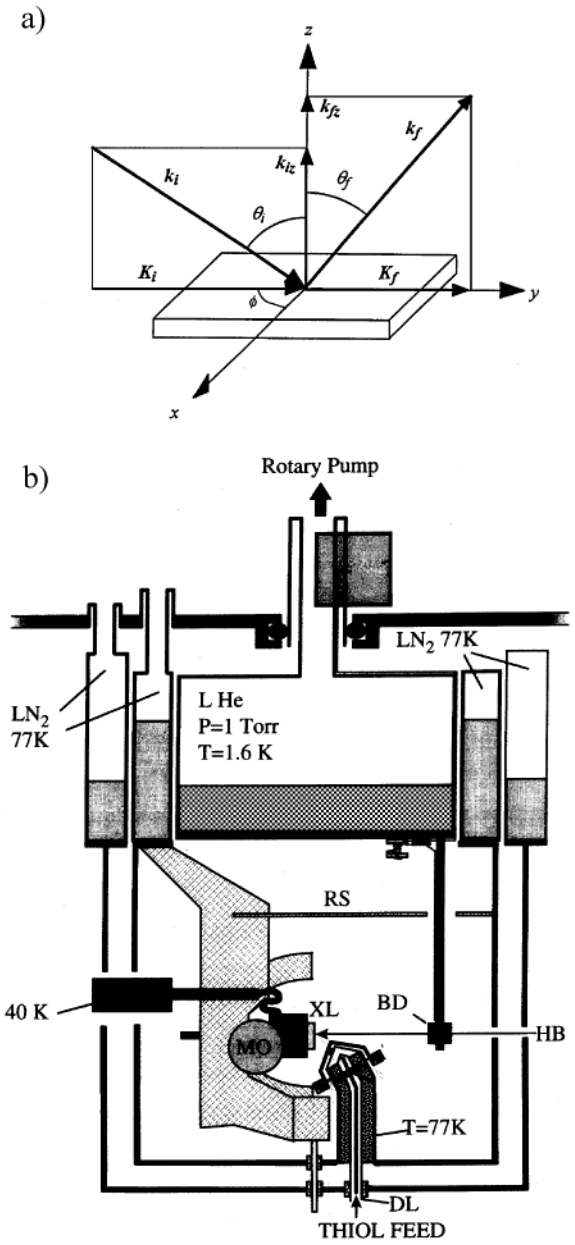

Figure 1. (a) Schematic representation of diffraction geometry. During measurements, the incidence angle θ_i is kept constant at 60 ± 0.5°, and the detector is rotated in the scattering plane, which is defined by the incident beam, surface normal and detector. Parallel momentum transfer, $\Delta K_{||}$, is equal to $K_f - K_i$. (b) Schematic of the inner part of the helium atom diffraction apparatus (RS, radiation shield; DL, dose line; HB, incident helium beam; XL, crystal; BD, bolometer detector).

The Au(111) surface was cleaned under ultrahigh vacuum through several sputter−anneal cycles (15−30 min) with an Ar pressure of $(1.3-1.5) \times 10^{-5}$ Torr and an Ar^+ energy of 1.0

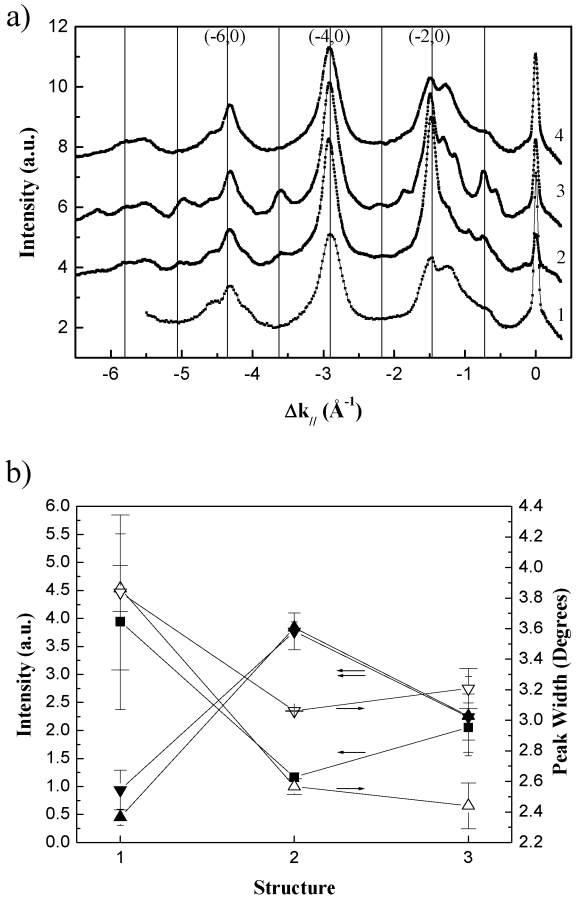

Figure 2. (a) Evolution of surface structure for various exposure and annealing periods as detailed in the text. Scans were taken along the gold nearest-neighbor direction ($\phi = 0°$). Expected diffraction peak positions of the $(3 \times 2\sqrt{3})$ superlattice are indicated by lines. (b) Specular intensity (■) (multiplied by 10 000) and the (−2, 0) (▲) and (−4, 0) (▼) peaks normalized to the specular signal. The widths of the (−2, 0) (△) and (−4, 0) (▽) peaks are also shown. The reported values are the averages of several scans reproduced in different set of measurements.

keV. The cleanliness of the surface was verified by the observation of the (0, −1) diffraction and $(23 \times \sqrt{3})$ reconstruction peaks of Au(111). Self-assembled monolayers of dimethyl disulfide were prepared by deposition from the gas phase through the doser shown in Figure 1b. The dimethyl disulfide was purified by several freeze−pump−thaw cycles prior to deposition. The molecular flux, *f*, on the crystal surface was determined from the 1/e decay time, τ, of the specular signal (the sticking coefficient was assumed to be unity) by use of the equation

$$f = (\sum \tau)^{-1}$$

where $\sum$ is the effective cross section of dimethyl disulfide,[29] which was assumed to be ∼165 Å^2.

Results and Discussion

Diffraction scans, taken along the $\langle 1\bar{1}0 \rangle$ direction ($\phi = 0°$) after different DMDS dosing and annealing procedures, are shown in Figure 2a. Curve 1 was obtained after exposing the gold surface kept at 200 K to a flux of $\sim 5 \times 10^{13}$ molecules cm^{-2} s^{-1}, which corresponds to 0.33 langmuir/s for 100 s followed by annealing at 330 K for 100 s. The $(\sqrt{3} \times \sqrt{3})$-R30° hexagonal peaks at 1.45, 2.90, and 4.36 Å^{-1} [(−2, 0), (−4, 0), and (−6, 0) peaks of the $(3 \times 2\sqrt{3})$ superlattice] are clearly visible in this curve (hereafter referred as structure 1). In addition,a few more peaks can be identified around the (−2, 0) and (−6, 0) peaks that are indications of a larger unit cell. However, these peaks are not well-resolved because of the small domain sizes. To ensure complete surface coverage, a second dosing was performed after the annealing. During this second dosing process, the surface temperature was ramped from 200 to 275 K for a total deposition period of ∼7 min. After this dosing, the sample was annealed at 320 K for 10 min, and the second curve of Figure 2a (structure 2) was obtained. Although the larger unit cell peaks were well-resolved, it was still impossible to determine the peak positions precisely enough for a structure determination. To increase further the domain size, the film was kept at 290 K overnight. A diffraction scan taken after this period is shown in the third curve of Figure 2a (structure 3) where the larger unit cell peaks are well separated from the hexagonal peaks. To further investigate the evolution of the system as a function of annealing time and temperature, we annealed the surface at 330 K for 15 min. As can be seen from the fourth curve in Figure 2a, this annealing process led to a structure that was identical to the first one. We then tried to optimize the deposition temperature and annealing temperature to obtain better resolution. The best results (well-resolved structure 3) were obtained by the procedure detailed above. We were not able to reach structure 3 by deposition of DMDS on the clean Au(111) surface without going through structure 1.

The diffraction characteristics of the above-mentioned three structures are summarized in Figure 2b. The higher specular intensity and peak width of structure 1 suggest that this phase is composed of small islands that do not cover the Au(111) surface entirely. We believe that the DMDS molecules deposited at 200 K stick where they land and cannot diffuse on the surface because of their low mobility at this temperature. This results in a random distribution of the molecules on the surface with a low packing density, which, before annealing, reduces the chance of incoming DMDS molecules will find free adsorption sites and cause coverage saturation. The packing density of the $(3 \times 2\sqrt{3})$ phase is 4.6×10^{14} thiolate molecules/cm^2. If the DMDS molecules are approximated as spheres with a radius of 4.6 Å (which is one-half of the van der Waals length of a DMDS molecule in the trans configuration) and are assumed to pack in a hexagonal lattice with a lattice constant of 9.2 Å, a packing density of 2.7×10^{14} thiolate molecules/cm^2 can be obtained. This suggests that adsorption at 200 K results in a surface coverage that is not more than 60% of surface coverage of the $(3 \times 2\sqrt{3})$ phase. Upon annealing to 330 K, the molecules rearrange and form domains of the $(3 \times 2\sqrt{3})$ superlattice, leaving a fraction of the Au(111) surface uncovered, which results in higher specular reflection. To predict the specular intensity as a function of surface coverage, the maximum attraction model proposed by Poelsema and Comsa[30] can be applied. According to this model, the specular intensity is given by the equations

$$I/I_0 = 1 - n_s U\Theta$$

for islands larger than the transfer width

$$I/I_0 = (1 - n_s U\Theta)^2$$

for islands smaller than the transfer width

where I_0 is specular intensity at zero coverage, n_s is the packing density of the substrate atoms, *U* is the unit cell size of the adsorbate, and Θ is the coverage. If the coverage for curve 3 is assumed to be 0.9 ML (we define 1 ML as the adsorbate density equal to one-third of that of gold atoms) and that of curve 1 to

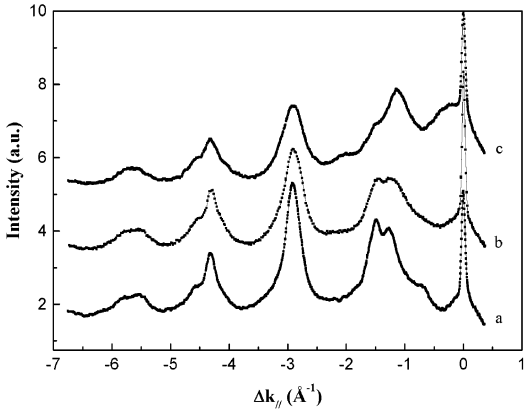

Figure 3. (a) Diffraction pattern obtained when structure 1 is annealed at 325 K for 15 min. (b) Diffraction pattern obtained when structure 1 is annealed at 330 K for 40 min. When this structure is annealed at 330 K for an additional 60 min, pattern c is obtained.

be 0.54 ML (60% of 0.9), a specular intensity ratio of 0.49 can be obtained by using the above-mentioned equations.[31] This value is in good agreement with the experimental intensity ratio of curve 3 to curve 1, which is ~0.5.

The average domain size depends on the migration to the steps of the so-called "etch pits",[15] which is a slow process that involves rearrangement of the positions of atoms of the substrate. This rearrangement of the substrate occurs rapidly only at temperatures at which this short-chain thiol can start evaporating. The annealing procedure can also introduce some disorder into the system and result in lower-density structures in addition to the $(3 \times 2\sqrt{3})$ superlattice domains. However, the broad feature of the diffraction pattern of structure 1 and the coincidence of the peak positions of these striped phases with those of the $(3 \times 2\sqrt{3})$ superlattice make it impossible for us to draw a certain conclusion about the arrangement of the organic overlayer. We believe that this relatively low-coverage phase (structure 1) acts as a nucleation center and that, upon further deposition, the $(3 \times 2\sqrt{3})$ phase grows from the preexisting islands. Increasing the dosing results in a higher packing density and the transformation of any existing striped phase to the denser $(3 \times 2\sqrt{3})$ structure. Upon further annealing, the domain size increases, which results in the better-resolved structure 3. The transformation of structure 3 back to structure 1 is caused by the desorption of the organic species during the annealing procedure at 330 K. If the annealing period is lengthened, the specularity of structure 1 increases, and new broad peaks near the specular appear, which we think is an indication of the increasing striped-phase coverage. This fact is clearly visible in Figure 3, where the change in diffraction pattern of structure 1 as a function of annealing temperature and period is shown. In previous LEAD[12,32] and LEED[33] studies on decanethiol, it was observed that high-quality samples kept their high-density $(3 \times 2\sqrt{3})$ superlattice form up to 350−370 K. Annealing the samples to higher temperatures resulted in several striped phases denoted as $(p \times \sqrt{3})$, where p indicates the distance between the stripes in units of the Au(111) nearest-neighbor distance. With increasing annealing temperature, the separation between the stripes increases and the $(3 \times 2\sqrt{3})$ phase disappears completely. The decrease in coverage was attributed to the desorption of the thiolate molecules during the annealing process. When the difference between the interchain interactions of longer- and shorter-chain alkanethiols is taken into account, it is reasonable to observe such phase transitions from a high-density $(3 \times 2\sqrt{3})$ phase to a lower-density structure at lower temperatures for films prepared using $(CH_3S)_2$.

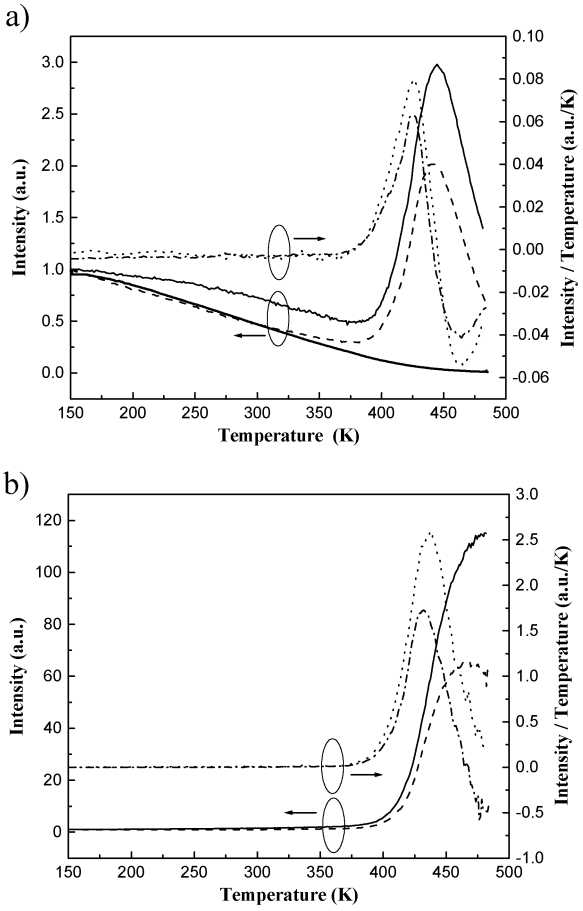

Figure 4. (a) Raw specular reflectivity data as a function of temperature for two different surface structures, structure 3 (—) and structure 1 (− − −), and the specular reflectivity of clean Au(111) (▬) that is used for sensitivity correction. Differentiation of specular reflectivity before sensitivity correction results in the dotted curve (· · ·) for structure 3 and the dash-dotted curve (− · − ·) for structure 1. (b) After correction for Debye−Waller attenuation and bolometer sensitivity, the solid (—) and dashed (− − −) curves are obtained for structures 3 and 1, respectively. Differentiation of these corrected data results in traditional TPD curves, dotted (· · ·) for structure 3 and dash-dotted (− · − ·) for structure 1. All of the curves except the raw specular reflectivities of structure 1, structure 3, and clean Au(111) are smoothed by adjacent-point averaging.

We also recorded specular reflection data as a function of crystal temperature to determine the desorption energies of the organic monolayers. The raw specular intensity data for structures 1 and 3 are shown in Figure 4a. It should be noted that these curves result from the change in surface coverage and the thermal motion of the surface molecules, so they are not a direct measure of desorbed species. However, the peak desorption temperatures that are needed to estimate desorption energies can still be determined after differentiation of the raw intensity data. The "traditional TPD" curves obtained by differentiation of the raw data (corrected for bolometer sensitivity changes and Debye−Waller attenuation) are also shown in Figure 4b. For these corrections, the temperature dependence of the specular reflection signal of the clean Au(111) surface was used (Figure 4a). The peak desorption temperatures were 432 ± 2 and 437 ± 2 K for structures 1 and 3, respectively. The corresponding desorption energy value determined after a Redhead analysis[34] assuming first-order desorption and using a preexponential factor of 10^{13} s^{-1} is 117 ± 3 kJ/mol. This value is very close to the previously reported chemisorption energies

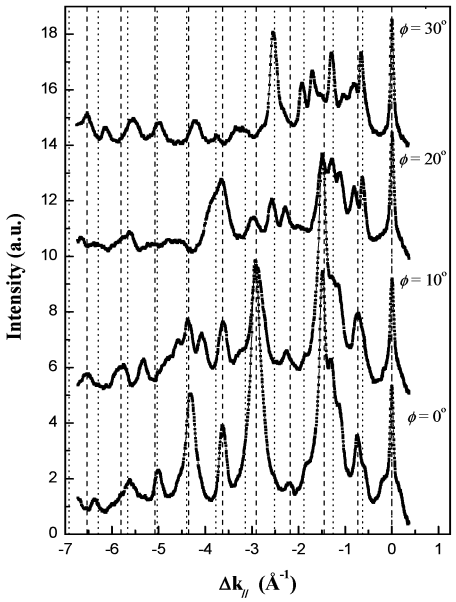

Figure 5. Diffraction scans taken along four different azimuthal angles. $\phi = 0°$ corresponds to the $\langle 1\bar{1}0\rangle$ direction, and $\phi = 30°$ corresponds to the $\langle 11\bar{2}\rangle$ direction. Expected positions of $(3 \times 2\sqrt{3})$ lattice points in the $\langle 1\bar{1}0\rangle$ $\langle 1\bar{2}0\rangle$ direction are indicated by dashed (dotted) lines.

for alkanethiols (126 ± 2 kJ/mol).[35] The difference might be caused by systematic errors.

The temperature dependence of the specular intensity before the start of desorption is a measure of the stiffness of the organic overlayer. Because the thermal motion of more rigid lattices will increase less rapidly with temperature than that of softer lattices, thermal attenuation of the specular intensity will be slower for rigid lattices. When the specular intensity variation of structure 3 with temperature was compared with that of structure 1, a slower decay could be observed. This observation leads to the conclusion that structure 3 is more rigid than structure 1, which is another support for the higher packing density of the former structure. At this point, we exclude the presence of physisorbed species either at the bare Au or on top of the $(3 \times 2\sqrt{3})$ domains. In a separate experiment, in fact, we deposited DMDS at 200 K on top of structure 1, and we observed a desorption peak at 237 ± 3 K. This temperature gives a desorption energy of 62 ± 2 kJ/mol, which is in good agreement with the bond additive model proposed by Wetterer et al. (69.8 ± 3.5 kJ/mol)[36] for the physisorption of hydrocarbons on Au(111). Because both structure 1 and structure 3 were measured after being annealed to ~300 K, they should involve only chemisorbed molecules.

To determine the unit cell of structure 3, we mapped the reciprocal space of this structure by taking diffraction scans at azimuthal angles, ϕ, between −25° and 95° (with respect to the gold nearest-neighbor direction $<1\bar{1}0>$, which is set to $\phi = 0°$) in 5° increments. Some representative scans are shown in Figure 5. For a better understanding of these curves, we should note, at this point, that the structure of our detector is designed to optimize the polar-angle (θ) resolution, whereas the resolution in the azimuthal angle (ϕ) is proportional to $\Delta K_{||}$ and can be as low as 40° for $\Delta K_{||} = 0.5$ Å^{-1}. (A more detailed discussion of this subject can be found in refs 28 and 29.) For this reason, at any given azimuth, off-azimuth peaks are also detected, especially for small $\Delta K_{||}$ values. This effect is clearly visible in Figure 5, where peaks between 0.6 and 2.0 Å^{-1} that belong to different azimuthal angles appear in all of the spectra. Another point is that, because of a small misalignment of the

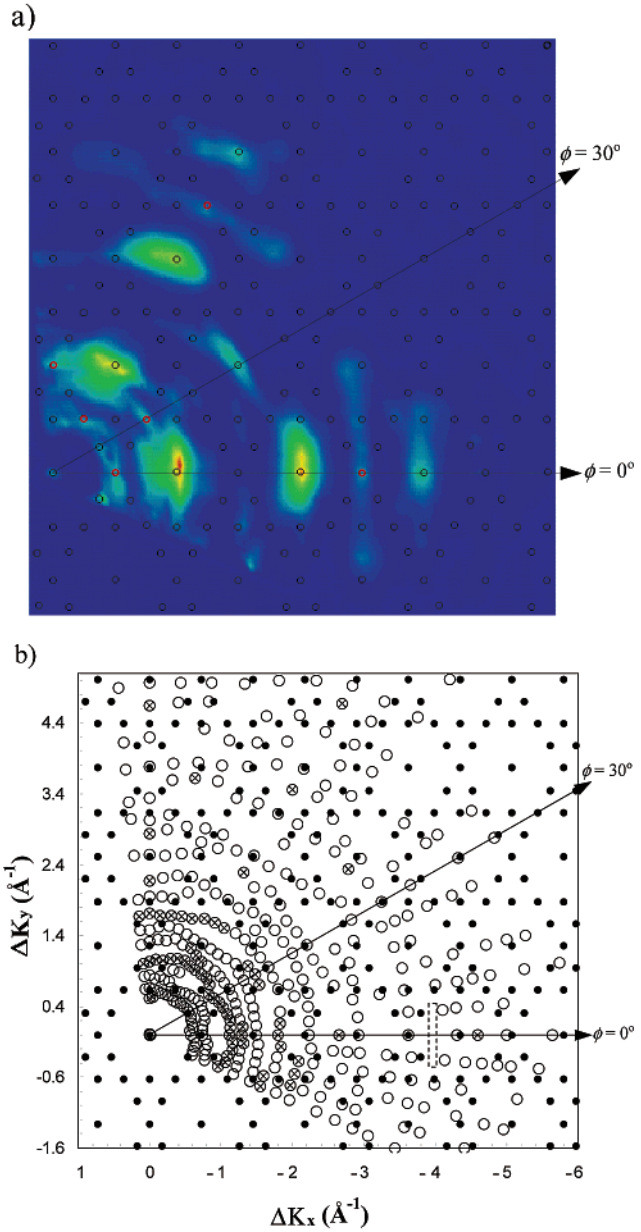

Figure 6. (a) Contour plot of diffraction scans taken in the range from −25° to 95°. Intensity increases from purple to red. (−1, 0), (−5, 0), and (0, −2) reciprocal lattice points are indicated by red circles; other $(3 \times 2\sqrt{3})$ lattice points are indicated by black circles. (b) Reciprocal-space plot of the experimental peak positions (○) in the same range as a. Calculated reciprocal space for the $(3 \times 2\sqrt{3})$ superlattice is indicated by ● symbols. It should be noted that experimental points (○) are not scaled to intensity. The experimental points that could not be assigned to any $(3 \times 2\sqrt{3})$ lattice point are shown by ⊗ symbols. The dashed box represents the resolution function of the apparatus.

center of rotation of the detector and the crystal, the deviation of the diffraction peaks from the expected positions increases as $\Delta K_{||}$ increases (peaks appear at smaller $\Delta K_{||}$ values as $\Delta K_{||}$ increases). In Figure 6a, we present a contour plot of the surface reciprocal space to make the above-mentioned facts more clear and to justify the peak assignments that will be made in the following discussion. As a complement to Figure 6a, a polar plot of peak positions, determined by fitting the diffraction scans to Lorentzians after a cosine background subtraction, versus azimuthal angle, ϕ, (which is equivalent to ΔK_x vs ΔK_y) is shown in Figure 6b. Both of the above-mentioned graphs are constructed on the basis of the ideal reciprocal space diagrams of the $(3 \times 2\sqrt{3})$ superlattice, which is the result of three

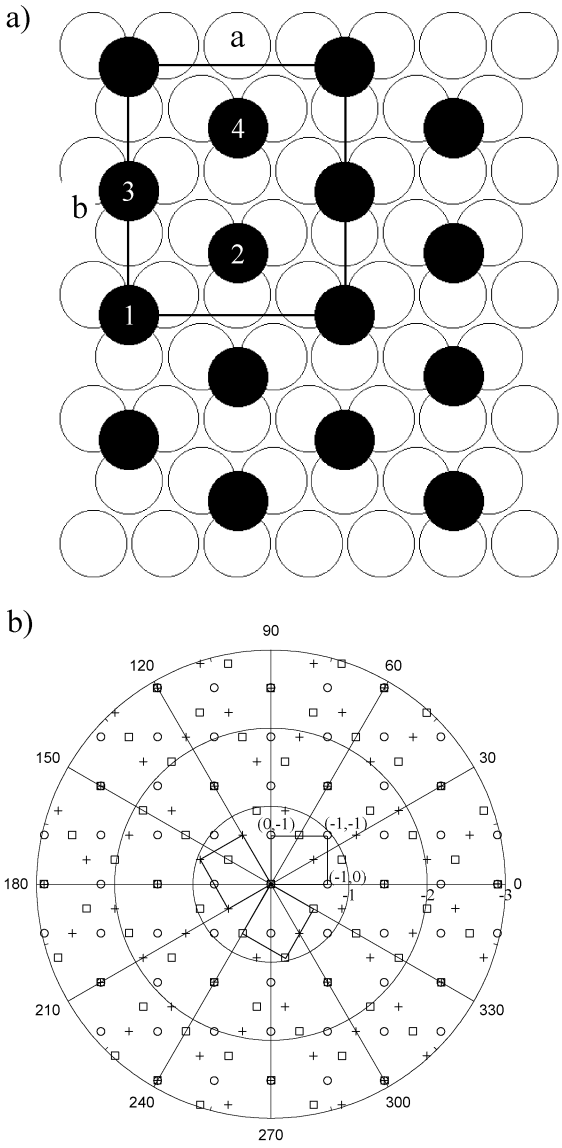

Figure 7. (a) Real-space representation of a $(3 \times 2\sqrt{3})$ unit cell. Open circles represent gold atoms, and filled circles represent thiolate molecules. The adsorption sites of thiolate molecules are not to be inferred from this figure. $a = 8.68$ Å, $b = 10.02$ Å. (b) Reciprocal-space representation of the $(3 \times 2\sqrt{3})$ structure. The expected diffraction pattern from three domains rotated by 120° with respect to each other are represented by open circles, open squares, and crosses. The three patterns coincide at the positions of the simple $(\sqrt{3} \times \sqrt{3})$-R30° lattice.

equivalent $(3 \times 2\sqrt{3})$ domains rotated by 120° with respect to each other. For the sake of clarity, real-space and reciprocal-space illustrations of these domains are shown in Figure 7.

It can be seen in Figure 6 that the diffracted peak positions fit quite well with the $(3 \times 2\sqrt{3})$ lattice points within the experimental limits. Most of the experimental points can be assigned to either an on- or an off-azimuth peak of the $(3 \times 2\sqrt{3})$ mesh. We compared several striped and centered unit cell structures with the experimental points, but none of these structures produced a better fit than the $(3 \times 2\sqrt{3})$ phase. An important feature that can be seen in Figure 6 is the appearance of the $(-1, 0)$, $(-5, 0)$, and $(0, -2)$ peaks, which should be forbidden according to the $(3 \times 2\sqrt{3})$ superlattice model proposed by Fenter et al.[10] for longer-chain alkanethiols. According to this model, in fact, molecules 1 and 2 in Figure 7a are identical, as are molecules 3 and 4. For these peaks to be observed, all of the thiolate molecules in the unit cell

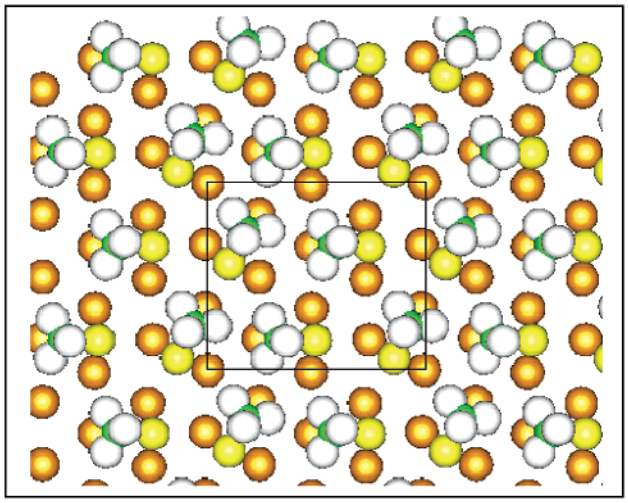

Figure 8. Full coverage $(3 \times 2\sqrt{3})$ unit cell structure proposed by Vargas et al.[22] Orange, yellow, green, and white circles represent gold, sulfur, carbon, and hydrogen atoms, respectively.

(molecules 1−4 in Figure 7a) should be inequivalent. This observation also allows us to discard the possibility of the formation of a striped $(3 \times 2\sqrt{3})$ phase as reported by Dishner et al.,[17] because, in their case, molecules 1 and 2 were identical and molecules 3 and 4 were missing. It is worth mentioning here that the STM images reported by Dishner et al.[17] greatly resemble the STM images of long-chain alkanethiols (rows of dark and bright spots). Whereas, for long chains, this pattern is thought to be caused by the height difference of the alternating rows or the different tilt angle of the alkyl chains, Dishner et al.[17] interpreted the dark rows as representing vacant sites, which is not a certain conclusion.

Deviations from the proposed $(3 \times 2\sqrt{3})$ structure were also reported by Camillone et al.[12] for decanethiol ($n = 10$) on Au(111). In their study, however, the observed intensities of these forbidden peaks were very small when compared with the intensities of the $(-2, 0)$ and $(0, -1)$ peaks, which was interpreted as reflecting a small distortion of the originally highly symmetric structure. In our case, the intensities of these peaks are comparable with the intensities of the $(-2, 0)$ and $(0, -1)$ peaks (Figure 6a), which indicates a higher distortion of symmetry. In Figure 8, the $(3 \times 2\sqrt{3})$ unit cell proposed by Vargas et al.[22] for methanethiolate on Au(111) is shown. In this structure, methanethiolate molecules occupy two different bridge sites, and they have the same symmetry as the unit cell proposed by Fenter et al.,[10] which does not agree with our observations. However, we should note that, in this calculation, dispersion forces between the carbon groups were neglected. It is possible that, when these forces are also considered, molecules 2 and 4 might deviate from their original positions to reduce the repulsive interaction. Such a distortion might lead to the observation of the originally forbidden peaks. Another explanation for the existence of the superlattice might be the formation of energetically favored gold vacancy defect sites during adsorption. This mechanism was recently proposed by Molina and Hammer,[37] who reported that the adsorption of methanethiolate onto a honeycomb structure with one gold missing for every three atoms present in the outermost Au(111) layer gives an improved account of the binding energy of the thiolate species. Because such a reconstructed substrate would be more corrugated than the perfect Au(111) lattice, it can yield a highly corrugated thiolate overlayer, which, in turn, can result in diffraction intensities of the superlattice comparable to the specular reflection, as in our case. Furthermore, as vacancy

formation is likely to be an activated process, this new possibility would also explain why thermal annealing is essential to the formation of the $(3 \times 2\sqrt{3})$ superlattice, especially when the hydrocarbon chains are short.

Conclusions

We have performed a study of the structural evolution of methanethiolate on the Au(111) surface by helium atom diffraction. Although we believe that the overlayer consists of small domains of the $(3 \times 2\sqrt{3})$ structure at lower surface coverages, we cannot dismiss the possibility of the existence of striped phases. Further dosing enhances surface coverage, and upon annealing at 290 K, a well-ordered $(3 \times 2\sqrt{3})$ phase can be obtained. Formation of the complete $(3 \times 2\sqrt{3})$ phase in a stepwise manner can be explained by the fact that, without annealing, it is not possible to achieve saturation coverage. Conversely, we found that annealing the sample at still higher temperatures (330 K) results in the transformation of the high-density $(3 \times 2\sqrt{3})$ phase to a lower-coverage phase that might be a mixture of $(3 \times 2\sqrt{3})$ and striped islands. This desorption temperature is reasonable in view of the fact that methanethiolate has smaller interchain interactions than the longer-chain thiols.[38] These results reveal that formation of the $(3 \times 2\sqrt{3})$ phase is a matter of sample preparation. Provided the right deposition conditions and annealing period for the system to reach equilibrium, there is no reason for it not to attain the $(3 \times 2\sqrt{3})$ superlattice, regardless of the chain length of the thiolate species. In view of the disagreement with the theoretical predictions of Vargas et al. and the new possibilities introduced by the work of Molina and Hammer, further theoretical work is highly desirable both to study the possible gold surface reconstruction and to analyze quantitatively our diffraction intensities.

The observed chemisorption and physisorption energies were in good agreement with the literature values. Observation of the peaks forbidden by the symmetry of the previous models indicates a larger distortion in the symmetry of the unit cell. The large number of diffraction channels caused by large surface corrugation of the $(3 \times 2\sqrt{3})$ phase hinders a simple quantitative analysis of the diffraction pattern. To account for the distortion of the unit cell and the surface corrugation, we are currently working on quasi-exact quantum mechanical calculation of the He diffraction intensities from a methanethiolate layer on Au(111).[39]

Acknowledgment. This work was supported by the DOE Materials Division under Contract DE-FG02-93ER45503. M.F.D. thanks Higher Education Board of Turkey for financial support. The authors thank Referee 65 for several useful suggestions.

References and Notes

(1) Ulman, A. *Chem. Rev.* **1996**, *96*, 1533.
(2) Schreiber, F. *Prog. Surf. Sci.* **2000**, *65*, 151.
(3) Scherer, J.; Vogt, M. R.; Magnussen, O. M.; Behm, R. J. *Langmuir* **1997**, *13*, 7045.
(4) Schon, J. H.; Meng, H.; Bao, Z. *Nature* **2001**, *413*, 713.
(5) Ulman, A. *An Introduction to Ultrathin Organic Films*; Academic Press: New York, 1991.
(6) Swallen, J. D.; Allara, D. L.; Andrade, J. D.; Chandross, E. A.; Garoff, S.; Israelachvili, J.; McCarthy, T. J.; Murray, R.; Pease, R. F.; Rabolt, J. F.; Wynne, K. J.; Yu, H. *Langmuir* **1987**, *3*, 932.
(7) Alves, C. A.; Smith, E. L.; Porter, M. D. *J. Am. Chem. Soc.* **1992**, *114*, 1222.
(8) Widrig, C. A.; Alves, C. A.; Porter, M. D. *J. Am. Chem. Soc.* **1991**, *113*, 2805.
(9) Dubois, L. H.; Zegarski, B. R.; Nuzzo, R. G. *J. Chem. Phys.* **1993**, *98*, 678.
(10) Fenter, P.; Eberhardt, A.; Eisenberger, P. *Science* **1994**, *266*, 1216.
(11) Fenter, P.; Eberhardt, A.; Liang, K. S.; Eisenberger, P. *J. Chem. Phys* **1997**, *106*, 1600.
(12) Camillone III, N.; Leung, T. Y. B.; Scoles, G. *Surf. Sci.* **1997**, *373*, 333.
(13) Schwartz, P.; Schreiber, F.; Eisenberger, P.; Scoles, G. *Surf. Sci.* **1999**, *423*, 208.
(14) Camillone III, N.; Chidsey, C. E. D.; Eisenberger, P.; Fenter, P.; Li, J.; Liang, K. S.; Liu, G. Y.; Scoles, G. *J. Chem. Phys.* **1993**, *99*, 744.
(15) Poirier, G. E.; Tarlov, M. J. *Langmuir* **1994**, *10*, 2853.
(16) Delamarche, E.; Michel, B.; Gerber, C.; Anselmatti, D.; Guntherodt, H. J.; Wolf, H.; Ringsdorf, H. *Langmuir* **1994**, *10*, 2869.
(17) Dishner, M. H.; Hemminger, J. C.; Feher, F. J. *Langmuir* **1997**, *13*, 2318.
(18) Voets, J.; Gerritsen, J. W.; Grimberge, R. F. P.; van Kempen, H. *Surf. Sci.* **1998**, *399*, 316.
(19) Yourdshahyan, Y.; Zhang, H. K.; Rappe, A. M. *Phys. Rev. B* **2001**, *63*, 081405(R).
(20) Gronbeck, H.; Curioni, A.; Andreoni, W. J. *Am. Chem. Soc.* **2000**, *122*, 3839.
(21) Hayashi, T.; Morikawa, Y.; Nozoye, H. *J. Chem. Phys.* **2001**, *114*, 7615.
(22) Vargas, M. C.; Giannozzi, P.; Selloni, A.; Scoles, G. *J. Phys. Chem. B* **2001,** *105*, 9509.
(23) Nuzzo, R. G.; Zegarski, B. R.; Dubois, L. H. *J. Am. Chem. Soc.* **1987**, *109*, 733.
(24) Ishida, T.; Motamoto, S.; Mizutami, W.; Motomatsu, M.; Tokumato, H.; Hokhari, H.; Azehera, H.; Fujihara, M. *Langmuir* **1997**, *13*, 3262.
(25) Heister, K.; Allara, D. L.; Bahnck, K.; Frey, S.; Zharnikov, M.; Grunze, M. *Langmuir* **1999**, *15*, 5440
(26) Noh, J.; Hara, M. *Langmuir* **2000**, *16*, 2045
(27) Farias, D. Autonomas University of Madrid, Madrid, Spain. Private communication, 2001.
(28) Camillone, N. Ph.D. Thesis, Princeton University, Princeton, NJ, 1994.
(29) Schwartz, P. Ph.D. Thesis, Princeton University, Princeton, NJ, 1998.
(30) Poelsema, B.; Comsa, G. *Scattering of Thermal Energy Atoms from Disordered Surfaces*; Springer-Verlag: Berlin, 1989.
(31) To calculate the decay in the specular intensity of curve 1, the second of the reported equations was employed because, in this case, the average domain size is smaller than the transfer width which is evidenced by the broad diffraction peaks shown in Figure 2. For curve 3 instead, the first equation was employed because the width of the (−2, 0) diffraction peak is equal to the instrument-limited width (∼2.2°) within the computational uncertainties. Actually, the peak widths shown in Figure 2b are broadened by the off-azimuth peaks and/or the tails of the neighboring on-azimuth peaks, which increases the uncertainty in the fitting procedure. The relatively high width of (−4, 0) peak of structure 3 is likely to be caused by the second kind of peaks, which, because of their very low intensities, could not be included in the fitting procedure.
(32) Camillone, N., III; Eisenberger, P.; Leung, T. Y. B.; Schwartz, P.; Scoles, G.; Poirier, G. E.; Tarlov, M. J. *J. Chem. Phys.* **1994**, *101*, 11031.
(33) Gerlach, R.; Polanki, G.; Rubahn, H.-G. *Appl. Phys. A* **1997**, *65*, 375.
(34) Redhead, P. *Vacuum* **1965**, *12*, 103.
(35) Lavrich, D. J.; Wetterer, S. M.; Bernasek, S. L.; Scoles, G. *J. Phys. Chem* **1998**, *102*, 3456.
(36) Wetterer, S. M.; Lavrich, D. J.; Cummings, T.; Bernasek, S. L.; Scoles, G. *J. Phys. Chem.* **1998**, *102*, 9267. The errors in this model can be as much as 8.6% for thiol molecules; the error given in the text is calculated by assuming an error of 5%.
(37) Molina, L. M.; Hammer, B. *Chem. Phys. Lett.* **2002**, *360*, 264.
(38) Nuzzo, R. G.; Dubois, L. H.; Allara, D. H. *J. Am. Chem. Soc.* **1990**, *112*, 558.
(39) We are collaborating with the group of D. Farias of the Autonomas University of Madrid, Madrid, Spain, and plan to address this problem again in a future publication.